www.springer.com/41230
https://doi.org/10.1007/s41230-023-3039-9



# To improve robustness of mechanical properties of semi-solid cast A356 alloy using taguchi design method

***Yi-wu Xu[1, 3], Hong-yi Zhan[2], Wei Tong[3], Jin-ping Li[4], Le-peng Zhang[4], De-jiang Li[1], and Xiao-qin Zeng[1]**

*1. School of Materials Science and Engineering, Shanghai Jiao Tong University, Shanghai 200240, China*

*2.China Science Lab, General Motors Global Research & Development, Shanghai 201206, China*

*3.General Motors (China) Investment Co., Ltd., Shanghai 201206, China*

*4.China International Intellectech Corporation (CIIC), Beijing 100004, China*

**Abstract:** Mechanical properties of semi-solid casting are dependent on multiple processing parameters, and improper processing parameters will not only reduce mean data but also increase variations. The present study investigated the impact of parameters in slurry preparation and heat treatment on the yield strength and ductility of T6 heat-treated A356 Al-Si alloy using rapid slurry forming (RSF) semi-solid casting. The focus was primarily on the robustness of mechanical properties based on Taguchi design method. By analyzing signal-to-noise ratio and minimum value calculated from $\bar{x}$-3$S$, the optimum slurry preparation parameters and heat treatment parameters were determined to be no quench, enthalpy exchange material (EEM) temperature of 140 °C, EEM-to-melt ratio of 6mass%, stirring time of 18 s, solution heat treated at 520 °C for 2 h, and ageing heat treated at 190 °C for 6 h. In a small batch validation, the –3$S$ yield strength and –3$S$ elongation reach 256.1 MPa and 5.03% respectively, showing a satisfactory robustness. The hardness and microstructure of heat-treated samples with the best and worst properties were characterized to gain insight into the underlying mechanisms affecting the mean value and variations of mechanical properties.

**Keywords:** semi-solid casting; taguchi design method; signal-to-noise ratio; mechanical property; microstructure

**CLC numbers:** TG146.21 **Document code:** A **Article ID:** 1672-6421(2024)02-175-10

## 1 Introduction

Mass reduction for automotive components has become one of the key approaches for greenhouse gas emission reduction of the automotive industry [1]. Materials selection, tooling design, and processing parameters are the three crucial pillars for achieving mass reduction in automotive castings [2]. Gravity casting and low pressure die casting processes have a relatively longer cycle time, and hence higher manufacturing cost for high volume production. Traditional high pressure die casting (HPDC) process has a much shorter cycle time, which is suitable for scaled production in the automotive industry [3]. However, some casting defects, such as gas porosities and shrinkage porosities in HPDC components, cannot be eliminated by heat treatment process. This put limitations on the mass reduction potential of HPDC Al components.

Semi-solid metal (SSM) casting can be categorized to thixo-forming and rheo-casting [4]. In rheo-casting, a slurry containing a certain fraction of pre-solidified spheroidal Al grains is prepared via mechanical stirring, grain refiner addition, and controlled fast cooling for subsequent high pressure die casting. While, in thixo-molding, an ingot will be re-heated to semi-solid slurry state and then processed to the desired shape via casting or thermal plastic deformation [4]. In comparison to conventional HPDC process, SSM casting process shows planer filling pattern with minimized gas entrapment due to the well-controlled viscosity of slurry, and components produced by SSM casting can be heat treated. In addition, employing partially solidified slurry is beneficial for reducing solidification shrinkage in die casting and forming a homogeneous and fine microstructure [5]. All the features of SSM casting impart the produced parts good mechanical properties [6-7]. As thixo-molding requires high cost equipment with complicated maintenance and has the limitations in

***Yi-wu Xu**

Senior Engineer. His research interests mainly focus on casting process development, problem solving of casting defects, and preventing automotive casting failures. To date, He has published 12 technical papers.

E-mail: yiwu.xu@gm.com

**Received: 2023-03-27; Accepted: 2023-08-28**

terms of the size and complexity of casting, rheo-casting has attracted significant interests from the automotive industry as a novel approach for mass reduction [8]. Rheo-casting process is more complicated compared to conventional HPDC process due to more casting parameters involved in the process. In addition, after solution heat treatment, blistering phenomenon tends to occur on the surface of HPDC components owing to the porosities caused by entrapped air during die casting [9]. Qi et al. [10] found that factors such as initial melt temperature, die temperature, and melt temperature in transfer ladle significantly affect the microstructure and mechanical properties of A356 alloy in a novel DCR (distributary-confluence runner) rheo-casting process. Kang et al. [11] investigated how factors such as stirring velocity, stirring duration, and other processing parameters affect microstructure and mechanical properties of 7075 Al alloy. Previous studies have primarily focused on mechanical properties, while neglecting the robustness (i.e., variations) of these properties. In real production, engineering teams must place significant emphasis on the robustness or -3$S$ values of a product's mechanical properties. Typically, the -3$S$ value of a specific mechanical property can be obtained using the following equations [12]:

$$Y = \bar{X} - 3S \tag{1}$$

$$\bar{X} = \frac{x_1 + x_2 + \ldots + x_n}{n} = \frac{\sum_{i=1}^{n} x_i}{n} \tag{2}$$

$$S = \sqrt{\frac{\sum_{i=1}^{n} \left(x_i - \bar{X}\right)^2}{n-1}} \tag{3}$$

where $Y$ is the -3$S$ value, $\bar{X}$ is the mean value, and $S$ is the standard deviation. To mitigate failure risks in casting components, the -3$S$ value calculated using Eq. (1) is typically applied in component design. Therefore, it is crucial to identify critical factors that influence the robustness of mechanical properties in casting components. There are various methods available for SSM casting, including RSF (rapid slurry forming), the use of a SEED (swirled enthalpy equilibration device), and GISS (gas-induced semi-solid) method, etc [13]. The RSF method involves stirring the melt with a small chunk of aluminum known as enthalpy exchange material (EEM) for melt cooling and slurry preparation. Factors that influence RSF include alloy chemistry, stirring velocity, superheat, and mass ratio of EEM to melt [14]. Compared to SEED and GISS methods, RSF exhibits low sensitivity to temperature, as well as fast cooling facilitated by enthalpy exchange in a short period. Sharma et al. [15] reported that under various conditions of grain refinement and modification, an increase in holding time of slurry resulted in larger and more spherical α-Al grains, while hardness decreases for the investigated A356 alloy. Östklint et al. [16] investigated the correlations between Al addition levels and grain size/solid fraction of Mg-Al alloys prepared with RSF method. They reported that with an increase in Al content, solid fraction and grain size increased while mass ratio of EEM to melt and superheat conditions remained constant. In fact, there are multiple factors affecting the mechanical properties of final product made by RSF method. Hence, it is challenging to achieve robust product quality by a simple experimentation design.

The objective of this study is to improve the reliability of tensile yield strength and elongation of the T6 treated A356 alloy produced using the RSF casting process. The Taguchi design method was utilized to optimize various process parameters, including alloy chemistry, stirring velocity, superheat of melt, mass ratio of EEM-to-melt, and heat treatment process.

## 2 Taguchi experimentation design

Taguchi method is an approach for experimental design and data analysis, which has been widely applied in industry [17]. In Taguchi design, loss function is applied to evaluate the degree of the result deviating from the expected value, and the largest signal-to-noise (S/N) ratio is applied to evaluate the variation. Target can be categorized into three types: the higher the better (HB), the lower the better (LB), and the nominal the better (NB). Though these 3 types own different equations for calculating S/N ratio, they all follow a principle that the largest S/N ratio indicates better robustness. It is known that S/N ratio of HB and LB is only dependent on $\bar{X}$. In contrast, the S/N ratio of NB is determined by both $\bar{X}$ and $S$, which coincides with the objective of this study ($\bar{X}$-3$S$) [17]. Therefore, in the present study, NB was selected as target for S/N ratio calculation via the equation below [17]:

$$S/N = 10\log\frac{\bar{X}^2}{S^2} \tag{4}$$

The details of controlling factors and noise factors for Taguchi experimentation design can be found in Tables 1 and 2. It is worth noting that for varied solution and ageing heat treatment temperatures, S, M and L levels corresponds to different holding times, as shown in Table 3. The selection of different levels for control factors are based on previous practices. The final L18 experiment design can be found in Table 4.

**Table 1: Details of controlling factors**

| | Controlling factors | Levels | | |
|---|---|---|---|---|
| | | 1 | 2 | 3 |
| 1 | Water quench | Yes | No | – |
| 2 | EEM temp. (°C) | 100 | 120 | 140 |
| 3 | EEM-to-melt ratio (mass%) | 6 | 7 | 8 |
| 4 | Stirring time (s) | 15 | 18 | 21 |
| 5 | Solution temp. (°C) | 505 | 520 | 535 |
| 6 | Solution time (h) | S | M | L |
| 7 | Aging temp. (°C) | 160 | 170 | 190 |
| 8 | Aging time (h) | S | M | L |

Table 2: Details of noise factors

| | Noise factors | Levels | |
|---|---|---|---|
| | | 1 | 2 |
| 1 | Pouring temp. (°C) | 665 | 675 |
| 2 | Casting pressure (MPa) | 70 | 80 |

Table 3: Heat treatment controlling factors

| Solution temp. (°C) | Solution time (h) | | | Aging temp. (°C) | Aging time (h) | | |
|---|---|---|---|---|---|---|---|
| | S | M | L | | S | M | L |
| 505 | 1.5 | 2.5 | 5 | 160 | 2.5 | 5 | 10 |
| 520 | 1 | 2 | 4 | 170 | 2 | 4 | 8 |
| 535 | 0.5 | 1.5 | 3 | 190 | 1.5 | 3 | 6 |

During the optimization process, it is desirable to achieve a high mean value and a high S/N ratio. When there is a contradiction between mean value and S/N ratio, S/N ratio has a higher priority. If the difference in S/N ratio between two designs is less than 2, it is generally considered that these designs have similar robustness. In such cases, the mean value of the designs becomes the selection criterion.

In the present study, the priority is given to tensile yield strength over elongation, based on the product requirements. Therefore, the sequence for optimizing parameters should prioritize the S/N ratio of yield strength, followed by the mean value of yield strength, then the S/N ratio of elongation, and finally the mean value of elongation.

# 3 Experimental

## 3.1 Sample preparation

The manufacturing process of tensile bars included alloy melt preparation, slurry preparation, die casting, and T6 heat treatment. The slurry preparation utilizing the RSF method included EEM preparation from A356, 1st stirring, and 2nd stirring. A Rhecomp-EEM equipment was utilized to prepare the EEM, utilizing the same melt as that used for the final casting. During the preparation of the slurry, the EEM was firstly immersed into the melt held in a pouring ladle. Subsequently, it was rotated by a motor ($M_1$), as shown in Fig. 1(a). During the

Table 4: L18 experiment design

| No. | Water quench | EMM temp. (°C) | EMM-to-metal ratio | Stirring time (h) | Solution temp. (°C) | Solution time (h) | Aging temp. (°C) | Aging time (h) |
|---|---|---|---|---|---|---|---|---|
| 1 | Yes | 100 | 6 | 15 | 505 | S | 160 | S |
| 2 | Yes | 100 | 7 | 18 | 520 | M | 170 | M |
| 3 | Yes | 100 | 8 | 21 | 535 | L | 190 | L |
| 4 | Yes | 120 | 6 | 15 | 520 | M | 190 | L |
| 5 | Yes | 120 | 7 | 18 | 535 | L | 160 | S |
| 6 | Yes | 120 | 8 | 21 | 505 | S | 170 | M |
| 7 | Yes | 140 | 6 | 18 | 505 | L | 170 | L |
| 8 | Yes | 140 | 7 | 21 | 520 | S | 190 | S |
| 9 | Yes | 140 | 8 | 15 | 535 | M | 160 | M |
| 10 | No | 100 | 6 | 21 | 535 | M | 170 | S |
| 11 | No | 100 | 7 | 15 | 505 | L | 190 | M |
| 12 | No | 100 | 8 | 18 | 520 | S | 160 | L |
| 13 | No | 120 | 6 | 18 | 535 | S | 190 | M |
| 14 | No | 120 | 7 | 21 | 505 | M | 160 | L |
| 15 | No | 120 | 8 | 15 | 520 | L | 170 | S |
| 16 | No | 140 | 6 | 21 | 520 | L | 160 | M |
| 17 | No | 140 | 7 | 15 | 535 | S | 170 | L |
| 18 | No | 140 | 8 | 18 | 505 | M | 190 | S |

1st stirring process facilitated by motor $M_1$, there was a rapid decrease in the temperature of the melt due to the formation of α-Al nuclei [Fig. 1(b)]. Following this, the 2nd gentle stirring process facilitated by motor $M_2$ was conducted to ensure the homogeneous distribution of these nuclei throughout the entire melt [Fig. 1(c)]. The slurry was then put into the shot sleeve of a Buhler 840-ton die casting machine to form tensile bars. The tensile bars were put into water within 15 s after being ejected from the movable die.

The melt composition in the holding furnace of casting machine was measured and the results can be found in Table 5. To eliminate variations caused by different die cavities, all the testing bars are from the same die cavity, as shown in Fig. 2(a). The dimensions of the tensile bar, as per ASTM B557 standard, are depicted in Fig. 2(b). The main processing parameters applied in the HPDC process can be found in Table 6.

Heat treatments were done in an electrically heated air-circulating chamber furnace with temperature deviation smaller than ±5 °C. Heat treatment was performed within two days after the completion of casting. The aging treatment was carried out immediately following the solution treatment.

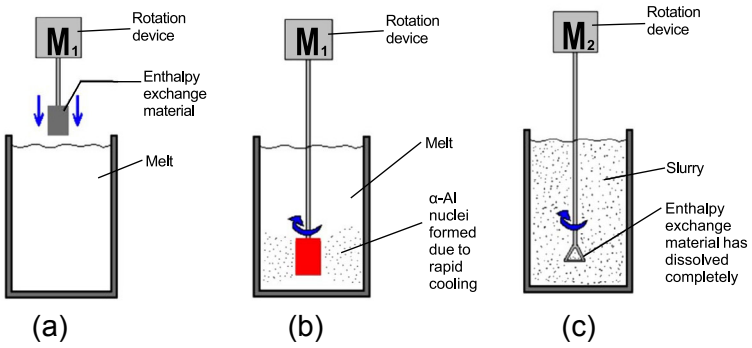


**Fig. 1: RSF slurry preparation: (a) EEM immersion; (b) 1st stirring; and (c) 2nd stirring**

**Table 5: Composition of the A356 alloy**

| Si | Cu | Fe | Mg | Mn | Zn | Ti | Al |
|---|---|---|---|---|---|---|---|
| 6.84 | 0.017 | 0.117 | 0.412 | 0.011 | 0.0196 | 0.136 | Bal. |

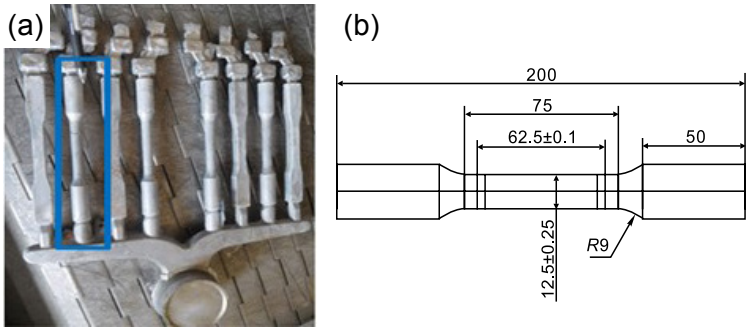


**Fig. 2: Obtained casting with the sampling location marked (a) and dimensions of tensile bar (mm) (b)**

### 3.2 Mechanical property testing and microstructural characterization

Specimens for microstructural observation were all firstly wet ground using silicon carbide papers, then mechanically polished and ultrasonically cleaned. Specimens for optical microscopy (OM) were etched using Keller's reagent (1% hydrofluoric acid, 2.5% nitric acid, 1.5% hydrochloric acid and 95% distilled water). Scanning electron microscopic (SEM) observations including energy dispersive X-ray spectrum (EDS) were performed on a Carl Zeiss AURIGA instrument equipped with Oxford EDX systems.

Hardness test was conducted on polished specimens using a Buehler VH3300 hardness tester with a load of 50 g and loading time of 10 s. The hardness data was averaged from 8–10 measurements. All the quasi-static tensile testing was conducted using an Instron 5982 tester at room temperature and a strain rate of $1\times10^{-3}$ $s^{-1}$. Three samples were tested for each condition.

## 4 Results and discussion

### 4.1 Taguchi design experiment results and analysis

Minitab software was employed to analyze the mean values and S/N ratios of yield strength and tensile elongation obtained in Table 7. These tests were conducted under the same conditions as presented in Table 4. Main effect plots for S/N ratio and mean value of yield strength and tensile ductility can be found in Fig. 3. The selection of optimum parameters can be explained as below:

(1) Quenching has the minimal impact on the S/N ratio of yield strength, but reduces mean yield strength by 5 MPa compared to not quenching, as shown in Figs. 3(a) and (b). Additionally, omitting the quenching process results in a 4-point increase in the S/N ratio of tensile elongation, and a slight decrease in the mean value of elongation by 0.2%. Therefore, it is preferable to avoid quenching castings after they are extracted from die cavity.

(2) EEM temperatures of 100 °C and 140 °C show similar impacts on S/N ratio and mean value of yield strength, and both are more beneficial than 120 °C, as shown in Figs. 3(a) and (b). Increasing EEM temperature from 100 °C to 140 °C improves the S/N ratio of tensile elongation by 2.4 and

**Table 6: Main processing parameters applied in HPDC**

| Holding temp. | Die temp. | Low speed | High speed | Shot sleeve heating temp. | Water temp. of quenching | Water quenching delay time |
|---|---|---|---|---|---|---|
| 670±5 °C | 220±20 °C | 0.20 m·s$^{-1}$ | 1.0 m·s$^{-1}$ | 170 °C | 30–50 °C | <15 s |

increases its mean value by 1.0%, as shown in Figs. 3(c) and (d). Therefore, an EEM temperature of 140 °C is preferred.

(3) An EEM-to-melt ratio of 6% shows the highest S/N ratio for both yield strength and tensile elongation. While the mean values of yield strength and tensile elongation under the condition of EEM-to-melt ratio of 6% are only slightly lower than the EEM-to-melt ratios of 7% and 8%. Hence, the optimum EEM-to-melt ratio was set to 6%, as shown in Figs. 3(a) and (c).

(4) There is a trade-off in the S/N ratio and mean value of yield strength and tensile ductility when selecting stirring time. As yield strength has a higher priority according to product requirement (strength critical), stirring time of 18 s is preferred.

(5) A solution temperature of 520 °C was selected as it imparts the highest S/N ratio and mean value of yield strength.

(6) A solution time of M level (2 h) was selected as its corresponding S/N ratio and mean value of elongation are the highest, and its corresponding S/N ratio for yield strength is also the highest. Moreover, the mean yield strength corresponding to M level is only slightly lower than that obtained with other levels.

(7) The ageing temperature was set to 190 °C considering its corresponding highest S/N ratio and mean value of yield strength.

(8) An ageing time of L level shows the highest S/N ratio

**Table 7: Taguchi design experiment results**

| No. | Mechanical properties | Pouring temp. 665 °C | | | | | | Pouring temp. 675 °C | | | | | |
|---|---|---|---|---|---|---|---|---|---|---|---|---|---|
| | | Casting pressure 70 MPa | | | Casting pressure 80 MPa | | | Casting pressure 70 MPa | | | Casting pressure 80 MPa | | |
| 1 | YS | 219.6 | 213.4 | 213.7 | 196.2 | 189.5 | 181.2 | 202.1 | 203.0 | 212.1 | 206.5 | 201.4 | 207.0 |
| | EL | 3.54 | 3.44 | 3.1 | 2.98 | 5.72 | 8.68 | 2.46 | 3.34 | 2.34 | 4.14 | 3.54 | 1.94 |
| 2 | YS | 228.6 | 227 | 228.7 | 240.3 | 233.7 | 232.9 | 236.1 | 233.9 | 246 | 241.7 | 235.3 | 242.9 |
| | EL | 2.18 | 2.86 | 0.58 | 3.40 | 1.72 | 1.42 | 2.64 | 6.96 | 4.26 | 3.50 | 4.18 | 1.94 |
| 3 | YS | 260.6 | 263.9 | 275.7 | 257.3 | 282.3 | 255.6 | 267 | * | 275.4 | 259.5 | 267.8 | 257.1 |
| | EL | 4.52 | 1.98 | 0.78 | 3.5 | 1.92 | 2.10 | 1.24 | * | 4.94 | 2.5 | 1.86 | 0.20 |
| 4 | YS | 260.1 | 269.8 | 259.9 | 264.7 | 266.2 | 263.4 | 255.7 | 259.2 | 262.1 | 265.4 | 256.3 | 254.8 |
| | EL | 2.50 | 3.82 | 4.12 | 6.20 | 0.62 | 2.96 | 2.06 | 2.86 | 3.12 | 1.90 | 4.18 | 3.76 |
| 5 | YS | 172.5 | 179.2 | 185.5 | 188.5 | 180 | 207.2 | 180.3 | 179.9 | 170.2 | 172.8 | 181.3 | 179.6 |
| | EL | 2.36 | 4.84 | 4.22 | 4.28 | 2.34 | 2.96 | 8.00 | 9.46 | 7.98 | 8.68 | 7.70 | 8.46 |
| 6 | YS | 232.6 | 229.9 | 226.2 | 162.2 | 140.0 | 112.6 | 253.0 | 247.9 | 250.8 | 248.6 | 255.5 | 248.6 |
| | EL | 4.24 | 3.54 | 4.48 | 5.36 | 3.78 | 3.96 | 3.06 | 3.58 | 2.56 | 3.92 | 3.06 | 2.92 |
| 7 | YS | 249.9 | 252.9 | 248.4 | 244.7 | 250.7 | 242.3 | 247.6 | 254.1 | 255.9 | 246.0 | 246.2 | 245.1 |
| | EL | 1.84 | 2.10 | 0.42 | 1.70 | 2.68 | 1.82 | 3.34 | 1.40 | 2.88 | 1.48 | 1.72 | 3.24 |
| 8 | YS | 243.9 | 243.6 | 247.1 | 235.8 | 246.0 | 239.4 | 243.3 | 237.6 | 226.4 | 198.1 | 212.1 | 218.1 |
| | EL | 2.44 | 1.32 | 2.78 | 4.78 | 2.34 | 2.58 | 4.76 | 2.44 | 2.58 | 4.40 | 4.34 | 3.06 |
| 9 | YS | 184.3 | 182.8 | 187.5 | 183.3 | 170.2 | 177.4 | 166.6 | 173.6 | 158.6 | 197.5 | 204.8 | 190.4 |
| | EL | 8.20 | 6.46 | 8.54 | 6.62 | 11.22 | 8.60 | 4.10 | 4.66 | 9.16 | 6.06 | 3.22 | 3.44 |
| 10 | YS | 187.7 | 195.0 | 176.7 | 196.3 | 180.9 | 197.1 | 191.4 | 207.4 | 180.3 | 194.6 | 190.8 | 200.3 |
| | EL | 4.60 | 1.66 | 3.48 | 3.24 | 3.10 | 4.10 | 4.88 | 4.88 | 4.60 | 5.16 | 4.78 | 0.60 |
| 11 | YS | 235.6 | 222.5 | 224.5 | 244.6 | 263.4 | 255.9 | 254.7 | 250.3 | 251.7 | 250.6 | 253.8 | 254.3 |
| | EL | 3.24 | 3.26 | 2.42 | 3.36 | 1.02 | 0.84 | 7.14 | 2.00 | 5.96 | 4.22 | 4.44 | 4.22 |
| 12 | YS | 231.0 | 240.9 | 226.5 | 229 | 224.8 | 220.9 | 241.6 | 235.4 | 231.2 | 232.1 | 225.2 | 234.7 |
| | EL | 3.36 | 2.96 | 5.36 | 0.92 | 4.06 | 1.36 | 1.30 | 1.64 | 1.66 | 1.80 | 3.50 | 2.02 |
| 13 | YS | 210.5 | 217.8 | 193.6 | 263.9 | 259.4 | 268.7 | 236.3 | 236.3 | 253.1 | 251.6 | 248.2 | 254.9 |
| | EL | 4.96 | 5.60 | 2.94 | 4.54 | 7.20 | 2.36 | 2.76 | 4.10 | 3.90 | 3.00 | 5.16 | 3.90 |
| 14 | YS | 241.1 | 244.2 | 243.4 | 222.8 | 230.8 | 220.2 | 240.4 | 241.9 | 239.8 | 231.0 | 235.9 | 237.0 |
| | EL | 2.52 | 3.16 | 1.28 | 2.16 | 1.14 | 5.66 | 3.96 | 4.96 | 4.9 | 1.68 | 2.00 | 3.78 |
| 15 | YS | 212.9 | 206.3 | 199.3 | 189.0 | 209.6 | 213.6 | 198.4 | 207.4 | 213.0 | 278.4 | 229.1 | * |
| | EL | 5.16 | 6.08 | 6.94 | 5.74 | 5.86 | 5.26 | 4.68 | 3.64 | 2.96 | 1.10 | 3.68 | * |
| 16 | YS | 229.1 | 232.1 | 230.3 | 235.3 | 232.1 | 242.0 | 241.4 | 244.8 | 240.3 | 241.4 | 244.5 | 237.0 |
| | EL | 5.50 | 5.40 | 5.48 | 4.10 | 0.68 | 5.12 | 3.00 | 3.56 | 4.38 | 3.38 | 4.96 | 0.72 |
| 17 | YS | 256.6 | 245.1 | 241.7 | 189.4 | 165 | 181.3 | 248.6 | 249.3 | 260.2 | 222.9 | 226.8 | 234.1 |
| | EL | 3.20 | 5.48 | 1.82 | 1.52 | 5.74 | 6.12 | 4.60 | 3.94 | 3.84 | 2.88 | 5.66 | 4.36 |
| 18 | YS | 250.0 | 247.1 | 248.4 | 240.3 | 237.2 | 241.2 | 242.8 | 243.3 | 246.4 | 239.0 | 244.8 | 238.0 |
| | EL | 3.92 | 4.36 | 4.34 | 3.10 | 5.06 | 2.84 | 3.36 | 5.88 | 3.02 | 2.34 | 3.50 | 0.38 |

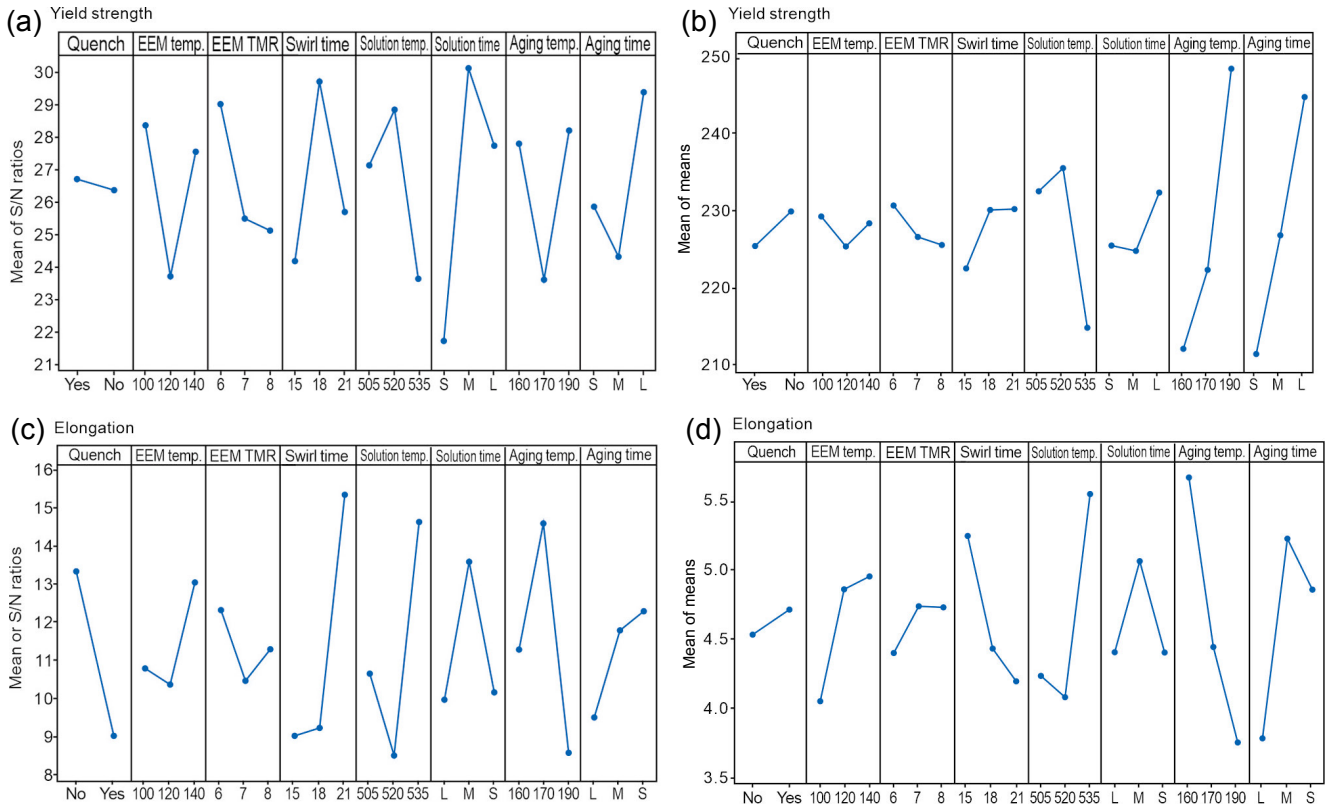


**Fig. 3: Main effect plots for S/N ratios (a and c) and mean values (b and d) of yield strength (a and b) and tensile elongation (c and d) (in which EEM TMR means EEM-to-melt ratio)**

and mean value of yield strength. In addition, the S/N ratio of elongation corresponding to ageing time of L level is also the highest and the corresponding mean value of tensile elongation is maintained at a high level. Hence, an ageing time of L level (6 h) is the optimum.

In summary, the optimized processing parameters are as follows: no quenching, stirring for 18 s the EEM that is pre-heated at 140 °C in the melt with an EEM-to-melt ratio of 6%, and then conduct a solution heat treatment for the obtained castings at 520 °C for 2 h followed by an ageing heat treatment at 190 °C for 6 h.

Using this set of optimum processing parameters as input, the mean value and standard deviations were predicted for both yield strength and tensile elongation. Predicted mean yield strength using Minitab software is 279.5 MPa, while the predicted mean elongation is only 2.01%, as shown in Table 8. By investigating and analyzing the low-ductility samples, it is found that the main reason responsible for the low ductility is that the 1st stirring induced a large number of carbides and oxides. This part is not the focus of current study, so the data was not included. After optimizing the 1st stirring operation by removing the coating agent from the stirring rod and adding a cover during water spraying EEM to reduce carbon and oxygen contamination, a small batch of 25 tensile bars were validated. The results indicate an average yield strength of 275.8 MPa and an average tensile elongation of 6.35%. The average yield strength is very close to the predicted value, with a deviation of only 3.7 MPa. The elongation is much higher than prediction. The minimal value of yield strength reaches 256.1 MPa, while the minimal value of tensile elongation reaches 5.03%.

**Table 8: Predicted values for tensile properties (UTS, YS, and EL) based on Taguchi design experiment and tensile properties obtained in a small batch validation**

| Tensile properties | Predicted | | | Experimental | | |
|---|---|---|---|---|---|---|
| | Mean | Stdev. | $\bar{X}$-3$S$ | Mean | Stdev. | $\bar{X}$-3$S$ |
| UTS | 312.6 | −0.22 | | 315.8 | 3.41 | 305.56 |
| YS | 279.5 | −11.24 | | 275.8 | 6.57 | 256.1 |
| EL | 2.01 | 1.0 | | 6.35 | 0.44 | 5.03 |

## 4.2 Hardness and microstructural characterization

### 4.2.1 Hardness

The selected samples for hardness testing and microstructural characterization include the sample with the highest yield strength referred as the best heat-treated sample B (UTS 305.5 MPa/YS 282.3 MPa/EL 1.92%), as marked in Table 7 by the green frame, the sample with the lowest yield strength referred as the worst heat treated sample W (UTS 280 MPa/YS 170.2 MPa/EL 7.98%), as marked in Table 7 by the red frame, and the optimal as-cast sample F (UTS 226.8 MPa/YS 99.5 MPa/EL 8.66%). No visible casting defects can be found in the fractured surfaces of these samples (Fig. 4). Five locations were selected along the radius direction for micro-hardness and microstructural characterizations, as shown in Fig. 5. The hardness of eutectic regions was averaged from 3 data points at each location while the hardness of the matrix was

tested once at each location. The hardness results are shown in Figs. 6(a) and (b) for eutectic region and α-Al matrix, respectively. For eutectic regions, as shown in Fig. 6(a), Locations 0 and 1 of Sample F which are near the surface show a relatively lower hardness (HV113.3 and HV117.6), while Location 4 of Sample F which is closest to the center of cross-section shows a much higher hardness over HV129, even higher than the hardness after heat treatment at the same location. After heat treatment, the hardness of Locations 0 and 1 is improved. The hardness of Locations 0 and 1 of Sample B is about 6–7 HV higher than the corresponding locations of Sample W.

The hardness of α-Al matrix is significantly increased after heat treatment. For the as-cast sample F, its hardness increases with the location moving from 0 to 3 along radius direction. For Sample B and Sample W, their hardnesses near the surface region (Location 0) are similar. However, at Location 1, α-Al matrix of Sample B (HV113.0) is much higher than that of Sample W (HV98.0), as shown in Fig. 6(b).

#### 4.2.2 Microstructure

From the optical observations presented in Fig. 7, it can be observed that eutectic Si exhibits a fibrous morphology in the as-cast microstructure (Sample F), but transforms into a spherical shape after heat treatment (Samples B and W).

#### 4.2.3 Elemental analysis

The contents of Mg, Si, Cu, and Fe in the matrix and eutectic region at Locations 0–4 in Fig. 5 were analyzed. The point elemental analysis was performed on three points at each locations for an average.

(1) In Sample B, Mg content increases from Location 0 to Location 1 in both eutectic region and the matrix. In contrast, in Sample W, the Mg content decreases from Location 0 to Location 1 in the eutectic region and the matrix. At Location 1, Mg content of Sample B in both areas is about 0.06% and 0.123% higher than those of W samples. In Sample F, almost no Mg detected in the matrix at Locations 0–4, while in the eutectic region, Mg content increases from Location 0 to Location 1 and then decreases from Location 1 to Location 4, as shown in Fig. 8.

(2) The concentration of Si in the matrix decreases from 5.07% at Location 0 to 1.68% at Location 1 in Sample B, while in the eutectic region, its concentration increases slightly from 22.23% to 26.49%, as shown in Fig. 8. In Sample W, the Si concentration in the eutectic region increases slightly from 19.85% to 20.66% at Locations 0 and 1, while in the matrix it remains similar. In Sample F, the Si concentration exhibits a similar trend to Sample W, with a moderate rise from 16.03% to 18.00% in the eutectic region at Locations 0 and 1, while remaining comparable in the matrix.

(3) In Samples B and F, the Cu concentration in both the matrix and eutectic regions remains similar at Locations 0 and 1. While for Sample W, the Cu concentration in the matrix decreases from 0.38% at Location 0 to 0.13% at Location 1, and in the eutectic region, it decreases from 0.28% at Location 0 to 0.19% at Location 1.

(4) In Sample B, the Fe concentration in the eutectic region increases from 0.34% at Location 0 to 0.78% at Location 1, while in the matrix, it remains almost unchanged. In Sample W, Fe concentration in the eutectic region increases from 0.35% at Location 0 to 0.59% at Location 1, while in the matrix, it decreases from 0.10% at Location 0 to 0.04% at Location 1. In Sample F, Fe concentration in both the matrix and eutectic regions remains similar at Locations 0 and 1.

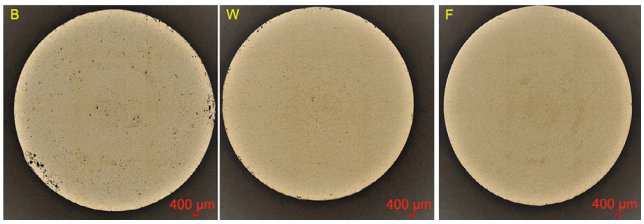


**Fig. 4: Macro-structures of cross-sections of Samples B, W and F near the fractured locations under optical microscope**

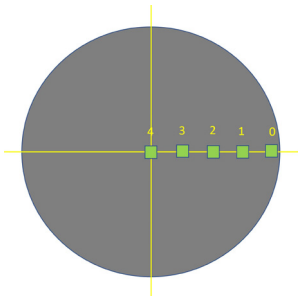


**Fig. 5: Sampling locations on cross-section for micro-hardness and microstructural characterizations**

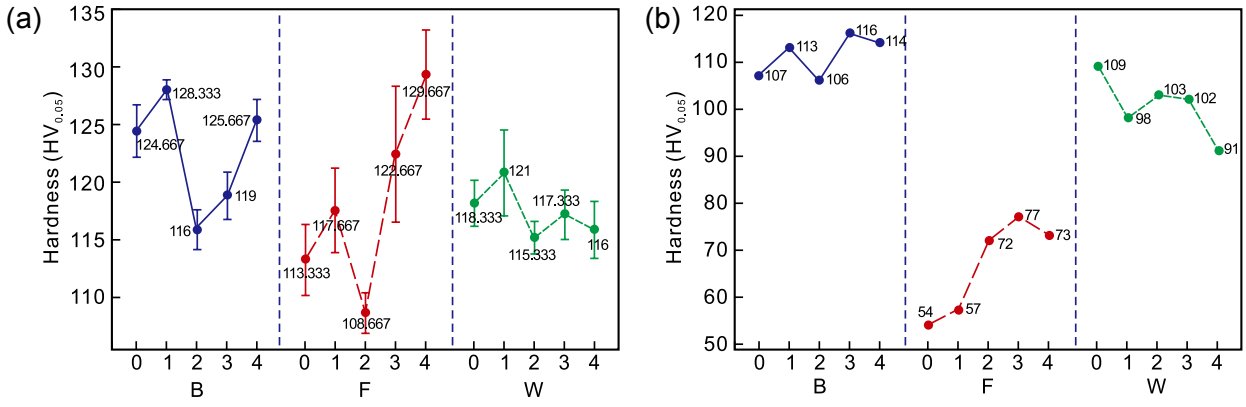


**Fig. 6: Hardness of eutectic regions (a) and α-Al matrix (b) at Locations 0–4 for Samples B, F and W**

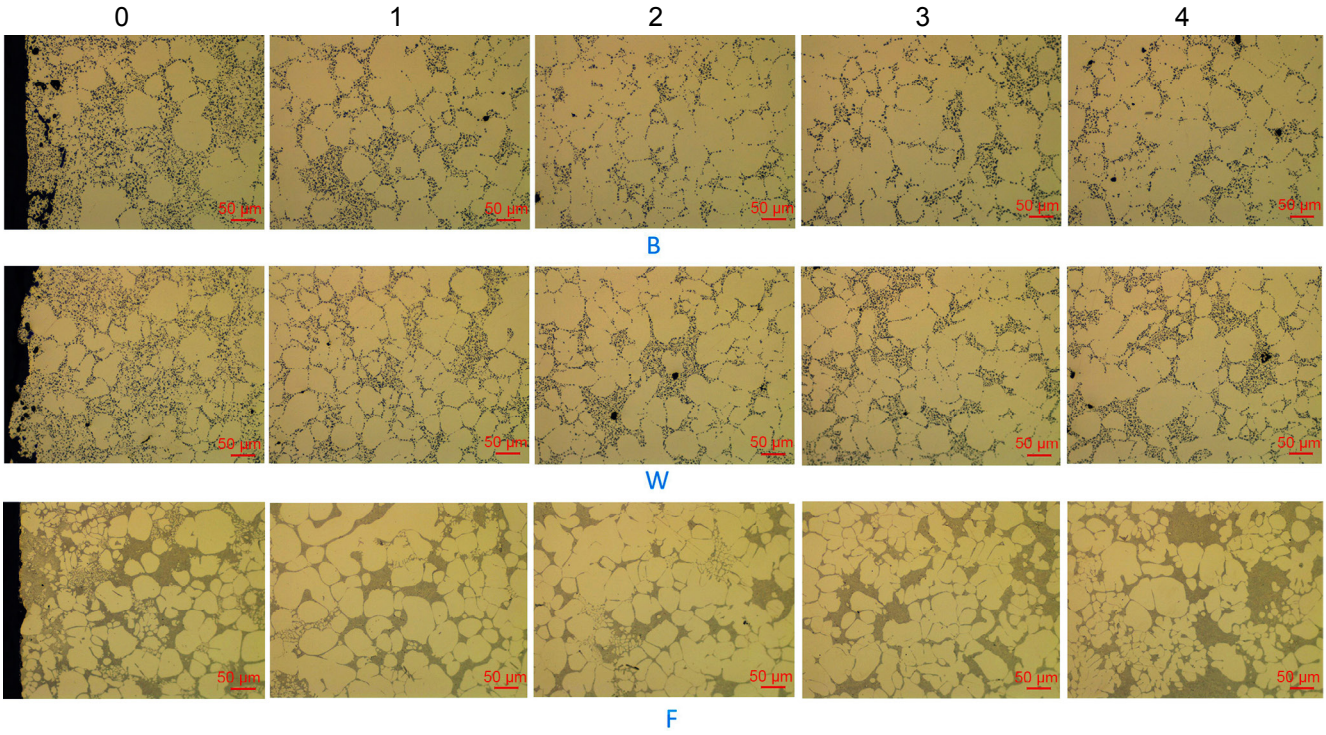


Fig. 7: Microstructures of Samples B, W and F along radius direction under optical microscopic observation

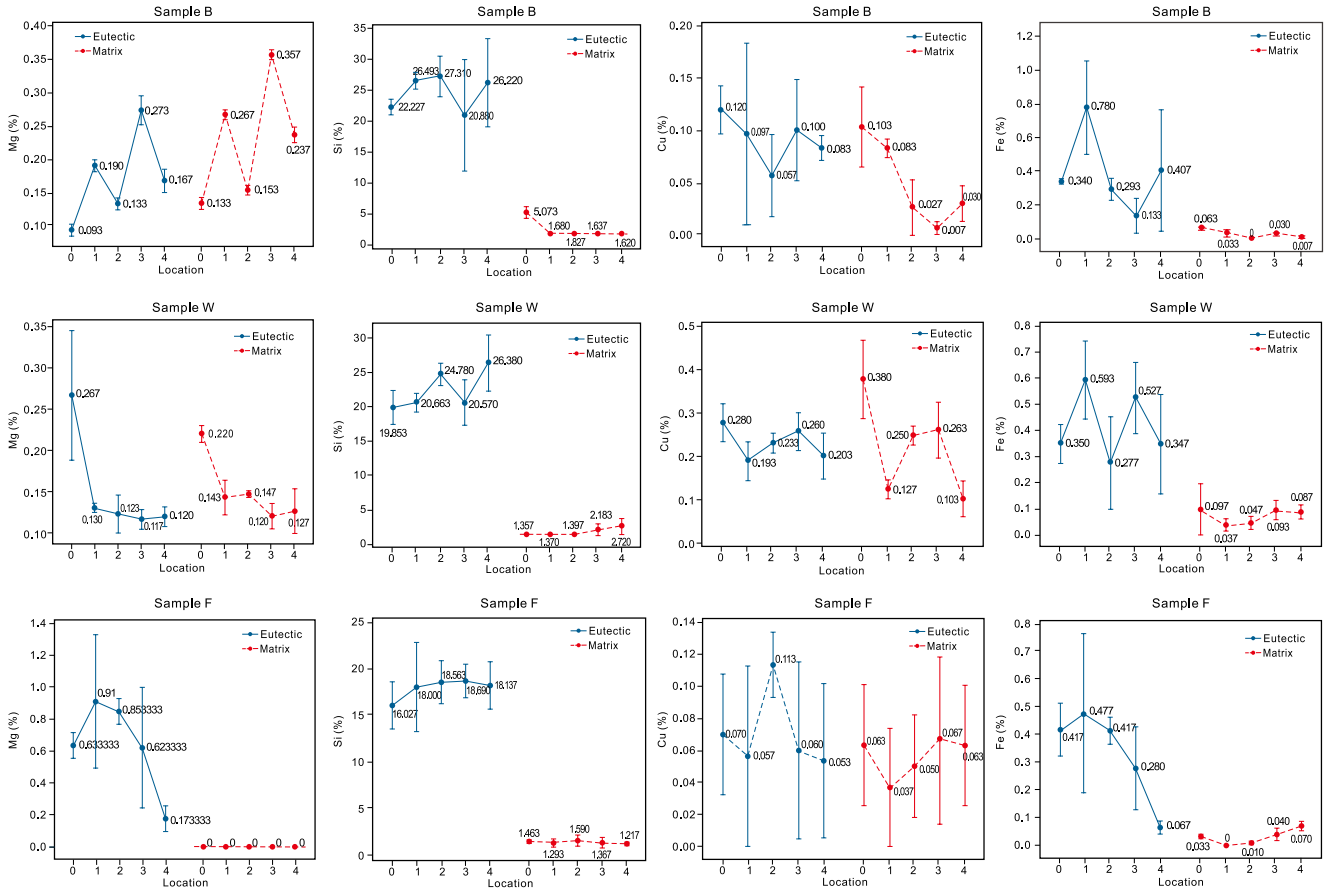


Fig. 8: Distribution tendency of Mg, Si, Cu, and Fe elements

## 4.3 Discussion

### 4.3.1 Effectiveness of Taguchi method

In Minitab 18, linear regression model was applied to build correlation between response and one or multiple independent variables. Assuming that the response is $Y$ and $x_1$ to $x_r$ are factors influencing $Y$, the linear regression model for row $j$ is shown below:

$$Y_j = \beta_0 + \beta_1 x_{j1} + \beta_2 x_{j2} + ... \beta_r x_{jr} + \varepsilon_j \quad (5)$$

where, $\varepsilon$ is random error and $\beta$ is regression coefficient.

In general, $R^2$ is used to evaluate the accuracy of prediction in relative to tested data. The equation for calculating $R^2$ is shown below:

$$R^2 = 1 - \frac{SS_{Error}}{SS_{Total}} \quad (6)$$

where, $SS_{Error}$ is the regression sum of squares and $SS_{Total}$ is the total sum of squares. In general, $R^2$ ranges between 0 and 1, and the larger value indicates a better prediction capability.

Take the mean value ($\overline{YS}$) and standard deviation ($S$) of yield strength in the present study as an example, their linear regression models are:

$\overline{YS}$=227.51-2.28 Quench_Yes+2.28 Quench_No+1.57 EEM temp._100-2.28 EEM temp._120+0.71 EEM temp._140+3.04 EEM TMR_6-1.03 EEM TMR_7-2.02 EEM TMR_8-5.09 Stirring time_15+2.54 Stirring time_18+2.55 Stirring time_21+4.94 Solution temp._505+7.92 Solution temp._520-12.85 Solution temp._535-2.05 Solution time_S-2.69 Solution time_M+4.74 Solution time_L-15.68 Aging temp._160-5.30 Aging temp._170+20.98 Aging temp._190-16.37 Aging time_S-0.87 Aging time_M+17.24 Aging time_L (7)

$S$=13.749-0.036 Quench_Yes+0.036 Quench_No-4.76 EEM temp._100+6.04 EEM temp._120-1.28 EEM temp._140-4.07 EEM TMR_6+0.18 EEM TMR_7+3.90 EEM TMR_8+2.33 Stirring time_15-4.71 Stirring time_18+2.38 Stirring time_21+1.31 Solution temp._505-3.43 Solution temp._520+2.11 Solution temp._535+9.13 Solution time_S-6.27 Solution time_M - 2.85 Solution time_L-4.83 Aging temp._160+7.03 Aging temp._170-2.20 Aging temp._190-1.59 Aging time_S+4.65 Aging time_M-3.07 Aging time_L (8)

In Eqs. (7) and (8), the coefficient of each variable indicates the contribution of the corresponding variable for output. Based on Minitab analysis, the $R^2$ value for mean yield strength prediction is 0.9404, which shows very high consistency. The $R^2$ value for standard deviation of yield strength is 0.9892 and the predicted standard deviation is −11.24 MPa. Though it deviates from the preset constraint ($S \geq 0$), it can be judged that the standard deviation is too low. This can also be validated in experimental results.

#### 4.3.2 Influence of microstructure and element distribution on mechanical properties

In comparison to the preparation of Sample W, the preparation of Sample B involved using a lower temperature (100 °C vs. 120 °C) of EEM, a higher EEM-to-melt ratio (8mass% vs. 7mass%), and a longer stirring time (21 s vs. 18 s). This resulted in the formation of a slurry with a higher solid fraction and a more homogeneous distribution of solid in liquid. Samples W and B experienced the same solution heat treatment (535 °C, 3 h), but Sample B experienced a higher ageing temperature (190 °C vs. 160 °C) and a longer ageing time (6 h vs. 2.5 h). As a result, Sample B exhibits a significantly higher yield strength compared to Sample W (283.3 MPa vs. 170.2 MPa in Table 8).

The yield strength of the as-cast sample F is only 99.5 MPa. However, after T6 heat treatment, the yield strength is remarkably improved due to the ageing-induced strengthening effect from the precipitation of $Mg_2Si$ phase. Based on the micro-hardness testing results, both the matrix and eutectic region of Sample B are apparently harder than those of Sample W at Locations 0 and 1. According to Fig. 6, a surface hardening case forms at Locations 0 and 1 after the T6 heat treatment. This increased hardness of the surface hardening case offers several benefits, including an improvement in the mean value of yield strength and a reduction in variations generated during production. In addition, the fraction of spheroidal precipitated phase formed in the intergranular region at Location 1 in Sample B is apparently higher than that at the same location in Sample W, as shown in Fig. 7, which may also explain the increased hardness at Location 1 after heat treatment.

In conventional die casting component, the skin layer that solidified at a very fast cooling rate will be supersaturated in Si and Mg elements [18]. Due to Magnus effect, the pre-solidified grains formed in the shot sleeve tend to flow away from surface region during the cavity filling [19]. In rapid slurry forming process, no chilled layer is formed in the sub-surface of casting coupon at Location 0, as shown in Fig. 7. Based on micro-hardness results in Fig. 6, the surface hardening effect mainly comes from eutectic region. Eutectic region consists of the matrix and multiple intermetallic phases including $Mg_2Si$, $Al_5FeSi$, and $Al_8Cu_6Mg_3Fe$ [20]. With an increase in Mg content, more $Mg_2Si$ will precipitate out to form dislocation which impedes the movement and deformation of crystals, thus improving the hardness [21]. It is found that the changing trend of Si content in the eutectic region at Locations 0 and 1 is similar as the evolution trend of hardness. In addition, the Mg content at Location 0 in Sample B is lower than that in Sample W but vice visa at Location 1. Hence, it is inferred that the Si concentration determines the surface hardening effect induced by ageing. Meanwhile, a high concentration of Mg at Location 1 has a synergistic effect on hardening along with Si. After solution heat treatment, Si particles in the eutectic region become spherodized [22], forming nano-sized $Mg_2Si$ precipitates in the subsequent ageing process [23]. Sample B experienced a higher ageing temperature (190 °C) and a longer ageing time (6 h) than Sample W, both of which significantly contribute to the desired ageing hardening effect.

## 5 Conclusions

(1) According to Taguchi method and its parameter filter criteria, the optimum parameters for the pursuit of the most robust yield strength and tensile elongation of semi-solid A356 alloy are as follows: no quench, EEM temperature of 140 °C, EEM-to-melt ratio of 6mass%, stirring time of 18 s, solution heat treated at 520 °C for 2 h, and ageing heat treated at 190 °C for 6 h. In a small batch validation, the −3$S$ yield strength and −3$S$ elongation reach 256.1 MPa and 5.03%, respectively, showing a satisfactory robustness.

(2) Locations 0 and 1 of Sample F, which are near the surface, show a relatively lower hardness in eutectic regions. After heat treatment, the hardness at Locations 0 and 1 of Sample B with a higher aging temperature and a longer aging time is slightly higher than the corresponding locations of Sample W. Eutectic Si transforms from fibrous morphology in as-cast state into a spherical shape after heat treatment. In addition, the changing trend of Si content in the eutectic region at Locations 0 and 1 is similar as the evolution trend of hardness.

(3) After T6 heat treatment, the strength of tensile bars is remarkably improved by forming a hardening case on the surface. During solidification of the slurry with a high solid fraction, the fraction of spheroidal precipitated phase in the eutectic region of surface is relatively higher, which contributes to the precipitation of more $Mg_2Si$ phase in the surface hardening case with the aid of an optimum heat treatment recipe. This will increase the mean value of yield strength, reduce the variation in yield strength, greatly improving $-3S$ value of yield strength.

## Acknowledgements

The authors would like to acknowledge the support and assistance from Mr. Li-qun Zhu from Kingpin Precision Industrial (Suzhou) Co., Ltd., as well as Mr. Hai-quan Zhang and Mr. Han-ming Cheng from Hongjin Metal Aluminum Co., Ltd.

## Conflict of interest

The authors declare that they have no known competing financial interests or personal relationships that could have appeared to influence the work reported in this paper.

## References

[1] Zhan H Y, Zeng G , Wang Q G, et al. Unified casting (UniCast) aluminum alloy–A sustainable and low-carbon materials solution for vehicle lightweighting. Journal of Materials Science & Technology, 2023, 154: 251–268.
[2] Luo A A, Sachdev A K, Apelian D. Alloy development and process innovations for light metals casting. Journal of Materials Processing Technology, 2022, 306: 117606.
[3] Vinarcik E J. High integrity die casting processes. John Wiley&Sons, Hoboken, 2002.
[4] Luo A A. Recent advances in light metals and manufacturing for automotive applications. CIM Journal, 2021, 12: 79–87.
[5] Seo P K, Kim H C, Kang C G. Numerical integration design process to development of suspension parts by semi-solid die casting process. Journal of Materials Processing Technology, 2007, 183(1): 18–32.
[6] Wang P, Liu J. Semi-solid processing thoery and technology of aluminum alloy. Beijing: Science Press, 2016: 2–13. (In Chinese)
[7] Zhang Z X, Chen T J, Liu K, et al. Efficient fabrication of semisolid nondendritic Al alloy slurry with high quality. China Foundry, 2022, 19(2): 117–130.
[8] Haga T, Kapranos P. Simple rheocasting processes. Journal of Materials Processing Technology, 2002, 130: 594–598.
[9] Hu X G, Zhu Q , Midson S P, et al. Blistering in semi-solid die casting of aluminium alloys and its avoidance. Acta Materialia, 2017, 124: 446–455.
[10] Qi M, Kang Y, Xu Y, et al. New technique for preparing A356 alloy semisolid slurry and its rheo-diecast microstructure and properties. Nonferrous Metals Society of China, 2021, 31: 1868–1884.
[11] Kang Y L, Li J Y, Li G N, et al. Preparation and rheological die-casting of 7075 aluminum alloy semisolid slurry. Journal of Net Shape Forming Engineering, 2020, 12: 3.
[12] Marilyn N M, Mary J B. What does it "mean"? A review of interpreting and calculating different types of means and standard deviations. Pharmaceutics, 2017, 9: 14. doi: 10.3390/pharmaceutics9020014.
[13] Winklhofer J. Semi-solid casting of aluminum from an industrial point of view. Solid State Phenomena, 2019, 285: 24–30.
[14] Ratke L, Sharma A, Kohli D. Effect of process parameters on properties of Al-Si alloys cast by rapid slurry formation (RSF) technique. Materials Science and Engineering, 2012, 27(1). doi: 10.1088/1757-899X/27/1/012068.
[15] Sharma S, Sharma A, Kumar S. Semi-solid forming of A356 Al alloy by rapid slurry forming process. In: Proc. 13th Internaitonal Conference on Aluminum Alloy, Pittsburgh, Pennsylvania, 2012.
[16] Östklint M, Wessén M. Microstructure characteristics and semi-solid slurry formation in binary Mg-Al alloys produced by the RheoMetal process. Solid State Phenomena, 2013, 192–193: 482–487.
[17] Krishnaiah K, Shahabudeen P. Applied design of experiments and Taguchi methods. PHI Learning Private Limited, 2012.
[18] Ji S, WangY, Waston D, et al. Microstructural evolution and solidification behaivior of Al-Mg-Si alloy in high-pressure die casting, Metallurgical and Materials Transactions: A, Physical Metallurgy and Meterail Science, 2013, 44(7): 3185–3197.
[19] Niu G, Wang J, Li J P, et al. The formation mechanism of the chill fine-grain layer with high supersaturation and its influence on the mechanical properties of die casting Al-7Si-0.5Mg alloy. Material Sceince & Engineering A, 2022, 833: 142544.
[20] Kaufman J G, Rooy E L. Heat treatment of aluminum castings, ASM handbook, 2011.
[21] Musa Y, Ozurek D. The effects of Mg amount on microstructure and mechanical properties of Al-Si-Mg alloys. Materials and Design, 2013, 51: 767–774.
[22] Long H C, Chen J H, Liu C H, et al. Microstructure evaluation during heat treatment for Al-7Si alloy. Journal of Chinese Electron Microscopy Society, 2013, 32(1): 18–24. (In Chinese)
[23] Colley L J, Wells M A, Poole W J. Microstructure-strength models for heat treatment of Al-Si-Mg casting alloys I: Microstructure evolution and precipitation kinetics. Canadian Metallurgical Quarterly, 2014, 53(2): 125–137.